High-temperature tensile cell for *in situ* real-time investigation of carbon fibre carbonization and graphitization processes

Michael Behr,[a]* James Rix,[b] Brian Landes,[a] Bryan Barton,[a] Gerry Billovits,[a] Eric Hukkanen,[a] Jasson Patton,[a] Weijun Wang,[a] Denis Keane[b] and Steven Weigand[b]

[a]Core Research and Development, The Dow Chemical Company, Midland, MI 48667, USA, and [b]DND-CAT Synchrotron Research Center, Northwestern University, APS/ANL 432-A004, 9700 South Cass Avenue, Argonne, IL 60439, USA. *Correspondence e-mail: mjbehr@dow.com

A new high-temperature fibre tensile cell is described, developed for use at the Advanced Photon Source at Argonne National Laboratory to enable the investigation of the carbonization and graphitization processes during carbon fibre production. This cell is used to heat precursor fibre bundles to temperatures up to ~2300°C in a controlled inert atmosphere, while applying tensile stress to facilitate formation of highly oriented graphitic microstructure; evolution of the microstructure as a function of temperature and time during the carbonization and higher-temperature graphitization processes can then be monitored by collecting real-time wide-angle X-ray diffraction (WAXD) patterns. As an example, the carbonization and graphitization behaviour of an oxidized polyacrylonitrile fibre was studied up to a temperature of ~1750°C. Real-time WAXD revealed the gradual increase in microstructure alignment with the fibre axis with increasing temperature over the temperature range 600–1100°C. Above 1100°C, no further changes in orientation were observed. The overall magnitude of change increased with increasing applied tensile stress during carbonization. As a second example, the high-temperature graphitizability of PAN- and pitch-derived commercial carbon fibres was studied. Here, the magnitude of graphitic microstructure evolution of the pitch-derived fibre far exceeded that of the PAN-derived fibres at temperatures up to ~2300°C, indicating its facile graphitizability.

1. Introduction

Carbon fibre exhibits a unique combination of extraordinary material properties, including high specific tensile modulus and strength, high-temperature creep resistance, excellent chemical resistance, high thermal conductivity, and low thermal expansion, that makes it an ideal material for structural reinforcement in light-weight composites. A wide range of applications have been fabricated using these carbon fibre reinforced polymer (CFRP) composites including aerospace and automotive structural components, wind-turbine blades, pressure vessels and sports equipment (Morgan, 2005).

The extraordinary combined properties of carbon fibres are a direct consequence of its constituent highly oriented graphitic microstructure. The fundamental building block of carbon fibre, a two-dimensional sheet of hexagonally arranged sp^2-bonded carbon atoms, is similar to that of graphene, which exhibits extraordinary mechanical properties (Oberlin, 1984). Specifically, a single sheet of graphene exhibits a tensile modulus of ~1010 GPa, tensile strength of 107 GPa, and 20% strain at failure (Zhao *et al.*, 2009). In carbon fibre, these
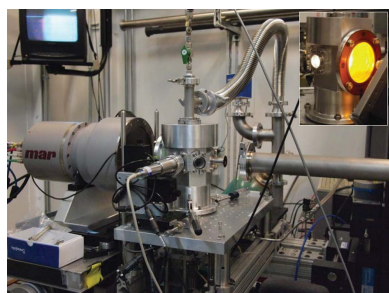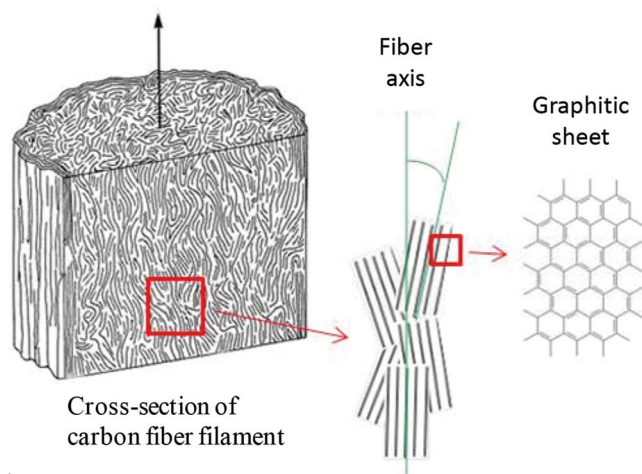
Figure 1
Pictorial representation of the aligned graphitic microstructure of a carbon fibre. Adapted from Morgan *et al.* (2005).

graphitic sheets are intertwined, well connected and preferentially aligned with the fibre axis, as shown pictorially in Fig. 1 (Johnson, 1987). Additionally, in-plane defects such as five- or seven-member rings are often present in high concentration. It is well accepted that this microstructure alignment controls the tensile modulus of the fibre. The degree of preferred orientation and the resulting tensile properties have been well studied by numerous groups using wide-angle X-ray diffraction (WAXD) for carbon fibres derived from polyacrylonitrile (PAN), mesophase pitch and cellulose precursors (Northolt *et al.*, 1991; Fischer & Ruland, 1980; Loidl *et al.*, 2003; Isaac *et al.*, 1994; Ruland, 1968; Huang & Young, 1995; Bacon & Schalamon, 1969).

Formation of this highly-aligned graphitic microstructure within carbon fibres is obtained through controlled pyrolysis of the stabilized precursor fibres. It is will known that the pyrolysis temperature and applied tension have a dramatic effect on the mechanical and structural properties of the resultant carbon fibres (Zhou *et al.*, 2011; Oberlin, 1984; Ogale *et al.*, 2002; Gao *et al.*, 2011; Perret & Ruland, 1970; Wu *et al.*, 2011; Isaac *et al.*, 1994). However, in order to investigate the impact of key manufacturing process parameters on microstructure development and to elucidate the structure–property–process relationships, a high-temperature fibre tensile device was designed and built, enabling the *in situ* investigation of the microstructure *via* WAXD during high-temperature carbonization and graphitization processes. Required functions for this device include the capability to (i) heat fibre bundles at variable ramp rates to temperatures relevant for carbonization/graphitization processes, up to 2400°C, (ii) heat both conducting and non-conducting fibres, (iii) apply tension to the fibre bundle to facilitate formation of highly-oriented graphitic microstructure while monitoring gauge length during heating, (iv) probe microstructure changes of the fibre samples during heating, and (v) conduct experiments in an inert atmosphere with <6 p.p.m. O_2, similar to that used in an industrial process, in order to minimize oxygen-induced fibre etching and defect formation. The apparatus, which is

described in detail herein, enables the rapid exploration and optimization of carbonization and graphitization processes. Additionally, this apparatus can be used to screen or develop new precursor stabilization processes, alternate chemistries, and various additive formulations based on their influence on microstructure development observed during high-temperature treatment.

The initial design concept for this apparatus was inspired by two previously reported high-temperature tensile devices used for studying *in situ* high-temperature creep behaviour (Rennhofer *et al.*, 2010), and thermomechanical properties (Sauder *et al.*, 2002, 2004) for PAN-, pitch- and rayon-derived carbon fibres. The apparatus of Sauder *et al.* (2002, 2004) demonstrated heating of single carbon filaments up to 2400°C by passing an electric current directly through the fibre. These filaments were attached to graphite grips using carbonaceous cement, and the entire assembly was maintained under vacuum. Tensile stress was applied during heating, and the thermomechanical properties and tensile behaviour of different fibre types were monitored as a function of temperature by stress–strain curves. The apparatus described by Rennhofer *et al.* (2006, 2010, 2014) was also used to heat and stress fibre bundles (up to 1700°C) in vacuum, but, in addition, they also monitored microstructure evolution as a function of time at ultimate temperature using WAXD. A laboratory X-ray source was used in the initial report, requiring relatively long (∼600 s) exposure times.

The high-temperature tensile device described in this work incorporates a number of novel design elements to more closely mimic typical commercial fibre carbonization and graphitization processes and to enable study of the entire process from stabilized precursor to final carbon fibre. A key novel element includes the ability to heat non-conductive stabilized precursor fibres, by using a radiative tungsten coil heating element, which enables the study of microstructure development during the initial low-temperature portion of the carbonization process. Additionally, this device was designed to be compatible with existing synchrotron experimental endstation infrastructure so that microstructure development could be monitored using WAXD with ∼1 s time resolution. Such time resolution enables experiments to mimic the fast temperature ramp rates utilized in actual industrial carbon fibre production processes.

2. Experimental apparatus and WAXD methodology

Figs. 2 and 3 show computer renderings of the high-temperature tensile device and photographs of the experimental set-up at APS with the various components identified. Briefly, the device consists of a large aluminium outer vacuum chamber equipped with dual quartz and polyimide windows mounted on a large metal plate. This outer chamber is easily removable and completely encloses the fibre heating and tensioning environment to provide a controlled vacuum or inert gas atmosphere during fibre heating. Fibre bundles are threaded down through the graphite clamps shown in Fig. 2, which are supported by the inner chamber, and electrically
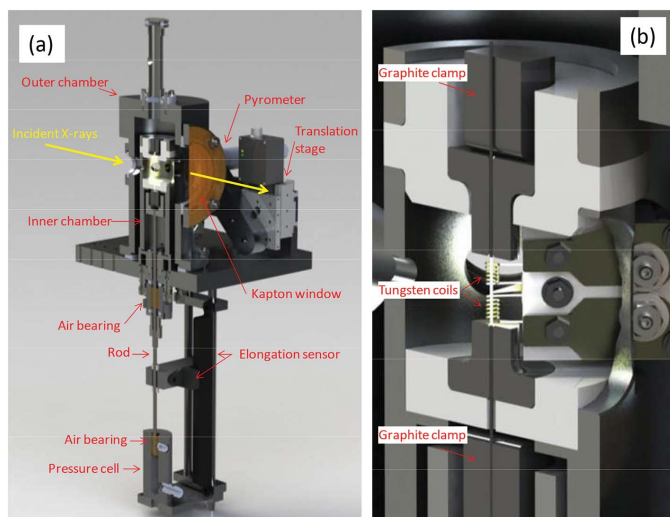
Figure 2
Computer renderings of the high-temperature tensile device showing a cross section of (a) the entire device and (b) the inner heating chamber.

insulated with large boron nitride disks. While the top clamp position is fixed, the bottom clamp moves vertically to enable application of stress to the bundle and accommodate changes in fibre length during the experiment. Heating of fibre bundles is achieved *via* one of two modes: (i) direct resistive heating by using the graphite clamps as electrodes to pass a DC current through the fibre bundle; or (ii) by passing a DC current through the surrounding tungsten coils to radiatively heat the middle section of the fibre bundle. A small side quartz window (shown in Fig. 3) enables the use of a digital pyrometer to monitor the temperature of the fibre bundle at a location coincident with the X-ray beam. Small- and large-area polyimide windows, respectively, on opposite-facing sides of the outer chamber, enable incident X-rays to enter and scattered X-rays to exit the chamber for real-time investigation of fibre microstructure development during a heating experiment. Operation of the device and process monitoring are controlled

remotely using *LabVIEW* (National Instruments); fibre strain is logged as a function of time, and temperature is logged and a mean value is calculated for each WAXD exposure.

2.1. Fibre heating

In order to enable heating of both conductive carbonized fibres and non-conductive precursor fibres, two different heating methods were employed. Conductive carbon fibres can be heated directly by passing a direct current through the fibre bundle using the graphite clamps as electrodes. This type of heating is variously referred to as Joule, Ohmic or resistive heating; the heat produced is proportional to the square of the current, $Q \propto I^2 R$, where Q is the heat released, I is the current and R is the resistance of the fibre bundle. The temperature achieved in the fibre by heating is a complex function of the heat capacity as well as various loss mechanisms. A typical power requirement to heat a $\sim$3000-filament bundle of carbon fibres to 2000°C is approximately 1200 W (72 V, 16.5 A). A Sorensen DCS 80-37 DC power supply is used to supply power for this heating mode. It was determined that a $\sim$3000-filament bundle was necessary to prevent premature failure at low temperatures; a combination of two $\sim$1500-filament bundles was also found to be acceptable. Electrical power is supplied between the bottom clamp through the steel rod external to the chamber, and the top clamp *via* a wire attached to the top fibre clamp hex screw (see Fig. 3).

Advantages of this direct heating method include the ability to: (i) achieve very high sample temperatures, >2300°C was the highest temperature observed, and (ii) uniformly heat the entire gauge length of fibre. Stabilized precursor fibres that were not conductive needed to be pre-carbonized to $\sim$900°C in nitrogen to produce a fibre that was conductive prior to *in situ* experiments. In a typical experiment, the heating profile was executed by increasing the voltage at a constant rate (typically $\sim$0.2 V s^{-1}), as controlled by *LabVIEW*. Fig. 4 shows experimentally-measured temperature ramps achieved using this heating method for two different commercial carbon fibres. These temperature *versus* time plots exhibit reasonable linearity up to high temperatures where radiative losses become significant. It should be noted that the slight deviation from linearity starting at $\sim$1500°C for the Thornel P25 fibre corresponds to the approximate onset of observed microstructure changes in orientation, interplanar spacing and crystal sizes, as shown in Fig. 14. This suggests that these microstructure changes have also resulted in a change in the intrinsic resistivity of the fibre.

In order to enable the study of lower-temperature microstructure changes, a secondary heating mode was designed to heat non-conductive precursor fibres. Specifically, the middle $\sim$1 cm of the

Figure 3
Photograph of the high-temperature fibre tensile device set up at APS in hutch 5ID-B. (a) Fully assembled (inset shows device in operation) and (b) inner chamber.
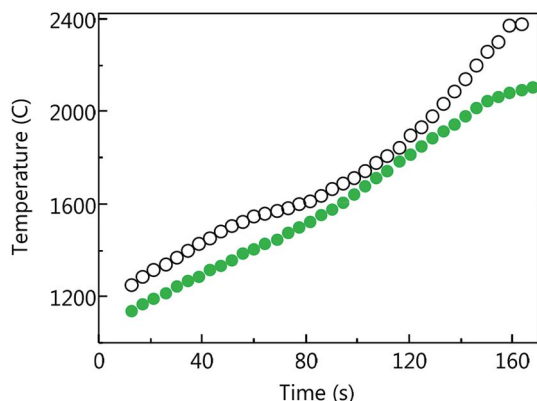
Figure 4
Temperature *versus* time plots for direct resistive heating of commercial carbon fibres: Hexcel IM-7 fibre (solid green symbols) and Thornel P25 fibre (open black symbols). A nominal $\sim$20 MPa stress was applied during heating.

fibre bundle gauge length was surrounded by a pair of tungsten wire coils connected in series; these coils are heated electrically, which in turn radiatively heats the fibre bundle. The power radiated by the coil is proportional to its surface area facing the fibre bundle and the temperature raised to the fourth power, $P_{Rad} \propto AT^4$, where A is the surface area of the coil and T is the temperature. The power required to heat the middle section of a $\sim$1500-filament bundle of carbon fibre to 2000°C is typically $\sim$420 W (24 V, 17.5 A). A Sorensen DCS 40-24 DC power supply is used to supply power. It should be noted that fibre bundles containing $\sim$1500-filaments, half the number used in direct heating, were used with coil heating in order to ensure that electrical shorts were not formed as a result of the fibre bundle contacting the surrounding coil. Also, the maximum voltage used was typically less than 15 V (corresponding to a fibre temperature of $\sim$1700–1800°C) in order to significantly extend coil lifetime.

Fig. 5 shows a photograph of the tungsten coil heating assembly with a magnified view in the inset. Two tungsten coils are wired in series and held in place with tungsten plates and molybdenum threaded rods, hex nuts and washers, which are electrically insulated from the inner chamber by a boron nitride plate. A small vertical gap along the fibre bundle, between the coils, was designed to accommodate the synchrotron X-ray beam and temperature measurement using the pyrometer. The total resistance of the wire is $\sim$0.4 Ω at room temperature. Electric power is supplied through two copper conductors that enter the chamber through the bottom plate, as shown in Fig. 3(*b*). Tin-coated braided copper wire is used to connect the coil assembly to the copper conductors as shown in Fig. 5. The materials of construction were carefully chosen to withstand the extreme temperatures experienced in this part of the cell for extended periods of time. Tungsten was chosen for its ability to be formed into a coil, and because of its high melting point of $\sim$3422°C. Molybdenum, which can be machined into threaded rods, nuts and washers, also exhibits a relatively high melting point of $\sim$2623°C. Fig. 6 shows a plot of temperature–time ramps for five replicate heating experi-
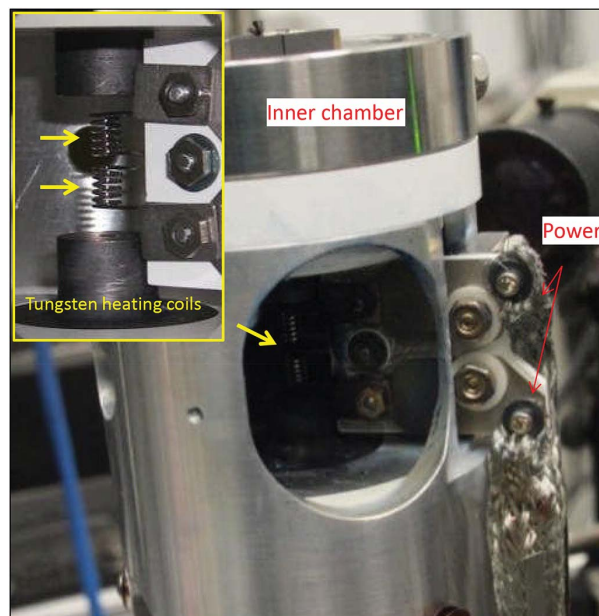
Figure 5
Photograph of the tungsten coil fibre heating assembly; the inset shows a magnified view.

ments, using oxidized PAN fibre, demonstrating the reproducibility of the heating technique.

2.2. Temperature measurement

The ability to accurately and precisely measure the temperature of the fibre bundle at the exact location where microstructure evolution is being monitored simultaneously *via* WAXD is critical to the operation of this high-temperature tensile apparatus. Due to the high operating temperature of the device, and the need to accommodate slight changes in fibre position for each run, a non-contact digital pyrometer was selected. The pyrometer used was an Exactus optical pyrometer made by BASF, which uses a measurement wavelength of 1550 nm to provide a temperature measurement range of 200–3000°C, with better than $\pm$0.45% accuracy. This
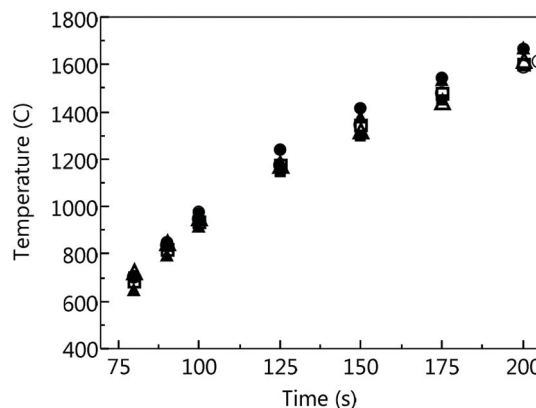
Figure 6
Five replicate temperature–time ramps achieved using a linear voltage ramp rate *via* tungsten coil heating (5 V min^{-1}) for oxidized PAN fibre.

device measures the temperature by using a photodiode to measure the energy of light emitted by the heated fibre bundle; this energy is proportional to the fourth power of temperature. An emissivity value of 1.0 was used for the black carbon fibre bundles studied in this work. The accuracy of the pyrometer temperature measurement was separately verified by comparing its temperature measurement of a fibre bundle heated using the tungsten coils with the known melting point of a thin metal wire threaded perpendicular through the fibre bundle. A multimeter was used to monitor the point when the metal wire melted, resulting in an open circuit. Two different metal wires were used: copper and platinum, which have melting points of 1085°C and 1768°C, respectively. In such experiments, the temperature measured by the pyrometer was within 2° of the expected melting point for each metal.

The optical pyrometer was mounted on a Zaber T-XY-LS13E-KT03 motorized XY translation stage. *LabVIEW* is used to control the translator to adjust the position of the pyrometer's focal spot using a laser accessory before each experiment to accommodate the exact position of the fibre bundle for each run. The optics of the pyrometer were custom fabricated to yield a measurement spot of less than 0.4 mm in diameter at a target distance of 75 mm. It is critical that the measurement spot size be smaller than the ~1 mm fibre bundle diameter to ensure that the pyrometer senses only the fibre surface to properly measure its temperature. The largest error in temperature measurement is due to minute changes in the position of the fibre, resulting in the pyrometer focal point moving slightly off the fibre surface.

The temperature measured by this technique was a line-of-sight average and information about the temperature profile through the bundle cross section was not available. Nevertheless, temperature uniformity amongst the fibers is expected to be a function of both the heating mode and temperature range. For example, all fibres are expected to be heated similarly with direct heating since the same DC voltage potential is applied across all filaments. The degree of heat loss from the outer filaments at high temperatures is unknown, thus the temperature measured may represent a lower limit. Coil heating is expected to result in greater non-uniformity, with fibres located near the surface of the bundle to be hotter than those on the interior. However, the observed (not shown) similarity in microstructure evolution measured *versus* temperature for coil and direct heating modes suggests that these temperature non-uniformities are relatively minor.

2.3. Fibre clamping system

Fig. 7 shows detailed photographs and a schematic of the clamp system used to hold fibre bundles in place during heating experiments, with the main components identified. The clamping system was designed to (i) withstand prolonged high-temperature operation, (ii) prevent excessive fibre damage and (iii) enable electrical continuity through the system for direct fibre resistive heating.

Fibre bundles are threaded from the top of the chamber through a pair of bevelled solid graphite blocks which directly
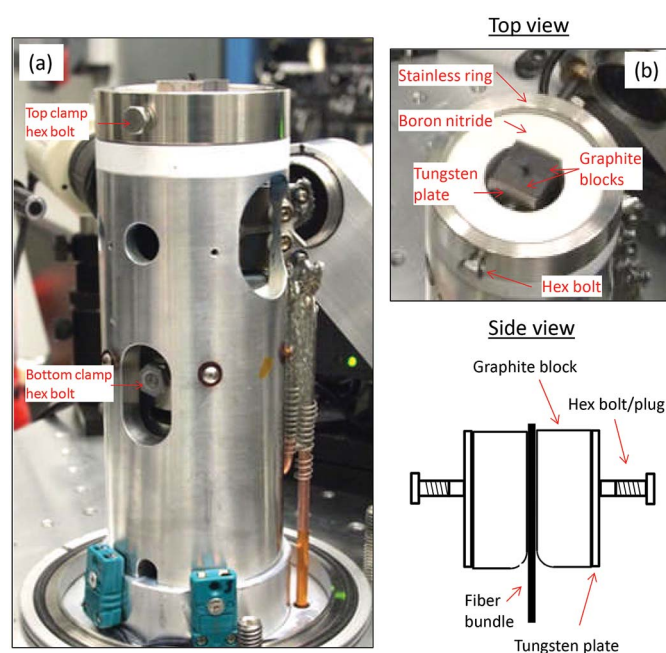
Figure 7
(*a*) Photograph of the inner chamber with top and bottom fibre clamp hex bolts labelled. (*b*) Top view and side view of the top fibre clamp components.

contact the fibre bundle. Both the top and bottom clamp assemblies are identical in the way the fibre bundle is held. The outer face of each graphite block is covered with a protective tungsten plate; molybdenum hex bolts threaded into opposite sides of the inner chamber can be tightened to push cylindrical stainless-steel plugs against the tungsten plates to squeeze together the graphite blocks onto the fibre bundle. A bevelled edge machined into the inner edge of each graphite block helps to prevent excessive damage to the surface filaments of the fibre bundle. However, as an additional layer of protection, a thin flexible sheet of graphite foil, with thickness of 0.005 inches (GrafTech International), was wrapped around the portion of the fibre bundle compressed by the graphite blocks. All clamp assembly components are electrically conductive; each assembly is further electrically insulated from the inner chamber and bottom plate to enable resistive heating of the fibre bundle. Finally, in separate heating experiments (not shown), it was verified that fibres did not slip in the clamping system under an applied stress of 300 MPa, which is about ten times the stress level utilized in typical experiments.

Alignment of the individual filaments within the fibre bundle was critical to ensure that the measured orientation values were representative of the fibre microstructure. To achieve well aligned filaments, typically one clamp assembly was tightened first, and then the bundle was tensioned slightly by hand before tightening the second clamp assembly. This method resulted in relatively well aligned filaments. It should also be noted that the degree of graphitic microstructure orientation far exceeded the slight misalignment of individual filaments within a bundle.

2.4. Tensile stress application

The extraordinary tensile properties of carbon fibres are a result of their constituent highly-aligned graphitic microstructure. To achieve this high level of alignment, it is necessary to apply tensile stress to the bundle during both low- and high-temperature heating processes. Thus, the device described herein was designed with a moveable bottom clamp assembly to enable application of tensile stress, and to allow for the resulting changes in fibre gauge length. Fig. 8 shows a schematic and photograph of the bottom clamp assembly. Briefly, the bottom clamp is attached to a stainless-steel rod that exits the base of the inner chamber through a gas bearing purged with pressurized helium at ~80 psig (psig = pounds per square inch gage). The rod terminates in a PVC pressure cell equipped with a second gas bearing to enable frictionless movement of the clamp. Compressed nitrogen gas at ~80 psig is supplied to the bottom gas bearing, which also purges the chamber of the pressure cell. An air filter regulator attached to the exit port of the pressure cell (not shown) is used to adjust the pressure within the pressure cell to exactly balance the weight of the entire clamp assembly; typically this is ~20 psig. With the entire assembly balanced, tensile stress can be applied to the fibre bundle by adding small shim weights to the top of the PVC block attached to the middle of the steel rod, just below the electrical connection site, as shown in Fig. 8. This method enables application of a constant load throughout a heating experiment. The cross-sectional area of the fibre bundle was estimated from single filament diameter measurements using laser diffractometry. Typically 15 filaments were measured per bundle.
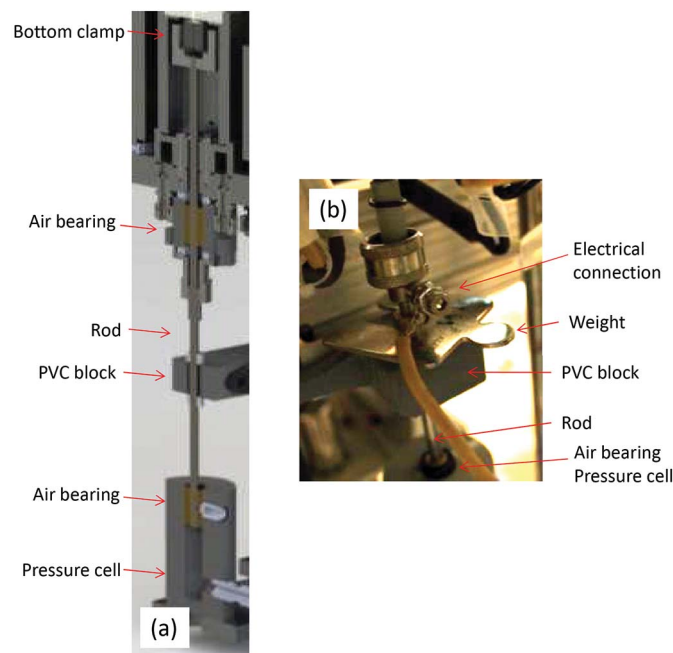
Figure 8
(a) Schematic view of the moveable bottom clamp assembly and (b) photograph of the PVC block with a metal weight used to apply stress to the fibre bundle.

Slight variations in the initial tension of filaments in a bundle may result in a slight non-uniform distribution of load. However, this distribution is expected to become more uniform with increasing temperature as elongation occurs. The level of non-uniformity is expected to be comparable with that achieved in typical industrial carbon fibre production processes.

2.5. Fibre strain measurement

Dimensional length changes of the fibre bundle, due to thermal expansion or chemical and/or physical changes, are monitored in real time using a non-contact position sensor. Changes in fibre gauge length are enabled by the free-sliding bottom clamp assembly, as shown in Figs. 2 and 8. Also shown schematically in Fig. 2 is the Honeywell SPS-L225-HALS magnetoresistive sensor bar mounted vertically below the chamber, parallel to the bottom clamp rod. This sensor detects the position of a magnet attached to the middle of the rod via a PVC block. Changes in fibre gauge length can be determined with a resolution of 0.14 mm, which corresponds to strain resolutions of ~0.25% and ~0.9% for direct and coil heating modes, respectively. This resolution is sufficient to detect major changes in fibre gauge length.

The zero point from which changes in gauge length were measured was set after weight application to the rod in order to account for system compliance. Thermal expansion of the fibre and graphite clamps was estimated and found to be insignificant (<0.3% strain).

2.6. Chamber atmosphere

Fibre bundles can be heated in either an evacuated chamber or with inert gas flow. A 67 L s^{-1} Pfeiffer Vacuum HiPace 80 turbomolecular pump was used to evacuate the chamber from the top port, which enables an ultimate pressure of ~5 × 10^{-4} torr to be achieved within ~5–10 min. There are two experimental limitations if heating is conducted in vacuum. First, the bottom clamp system cannot be moved due to the O-ring seal covering the air bearing, thus the fibres cannot be heated under stress. Second, it was observed that fibre bundles heated in vacuum broke prematurely at elevated temperatures, presumably due to the enhanced vaporization of carbon from the surface of the fibre.

The authors found it preferable to heat fibre bundles in an inert gas atmosphere, as this not only enables the application of stress but is also more representative of the actual carbonization and graphitization processes used in typical carbon fibre production processes. Nitrogen gas is typically used in high-temperature industrial ovens; however, due to the relatively high X-ray scattering cross section of nitrogen, it cannot be used during in situ WAXD experiments. Instead, ultra-high-purity (UHP) helium is used when in situ monitoring of microstructure with WAXD is needed. Further, it is critical that oxygen levels are sufficiently low to prevent oxidation and subsequent etching of the fibre bundle. Such reactions with oxygen form volatile CO_x species and result in defect formation and premature failure of the bundle. Typically, oxygen

levels less than 6 p.p.m. are desired; however, levels ~2 p.p.m. were routinely achieved by first evacuating the chamber before flowing UHP helium gas for ~5 min. Gas is supplied to the chamber directly through the top air bearing; the chamber is kept under a slight positive pressure by throttling the gas exiting the chamber through the top port that feeds the Advanced Micro Instruments, Inc., 1000RS-T2 oxygen sensor.

2.7. Wide-angle X-ray diffraction

The microstructure of carbon fibre bundles was monitored *in situ* and in real time during heating experiments using WAXD measurements conducted at the Advanced Photon Source (APS), DND-CAT, 5ID-B beamline. Fibre bundles were measured in transmission-normal geometry using the standard APS undulator X-ray source at 17 keV (λ = 0.7293 Å). The horizontal beam size was comparable with the bundle diameter, thus each measurement represents an average of all filaments within the bundle. The high-temperature tensile device was positioned such that the gap between the X-ray vacuum tube nose cone and the small polyimide window of the chamber was minimized, typically ~2 inches. Two-dimensional diffraction patterns were collected on a Rayonix MarCCD 2k × 2k camera with the acquisition time set at 1 s, and pixel binning of 2 (1024 × 1024 pixels). The detector readout time for 2 × 2 binning was ~4 s, thus a WAXD pattern could be collected every ~5 s. Angular calibration of the detector was conducted using a lanthanum hexaboride powder standard placed in a thin-wall capillary. The sample-to-detector distance was set such that the entire graphite (100) peak was captured, typically ~13 cm. Diffraction patterns were analyzed using the Dow-developed *SCATTER* data visualization and analysis package on the PV-WAVE platform (Rudolf & Landes, 1994), and *Jade* diffraction software. Graphitic microstructure orientation, average spacing between adjacent graphitic layers, and crystal sizes L_c and L_a were evaluated as a function of temperature during heating.

2.7.1. Microstructure orientation. The average orientation of graphitic layer plane normals relative to the fibre axis was evaluated indirectly from the azimuthal intensity distribution of the graphite (002) diffraction ring. Specifically, the intensity distribution of scattering from the (002) diffraction ring was evaluated relative to the meridional direction, yielding a $\langle\cos^2\delta\rangle$ orientation parameter (see Figs. 9 and 10). The $\langle\cos^2\varphi\rangle$ orientation parameter was then calculated using the relationship $\langle\cos^2\delta\rangle = 1 - 2\langle\cos^2\varphi\rangle$.

The intensity integrated across the specified 2θ range of the (002) diffraction peak was then extracted and plotted as a function of the azimuthal angle (φ = 0 to 360°), as shown in Fig. 11. The two peaks correspond to the two (002) diffraction peak maxima observed along the equatorial direction. Orientation parameters were numerically evaluated using the Dow-developed *SCATTER* data visualization and analysis package on the PV-WAVE platform over four regions: 90°–0°, 90°–180°, 270°–180° and 270°–360°, and then averaged to yield a single value. The 0° position corresponds to the 3 o'clock
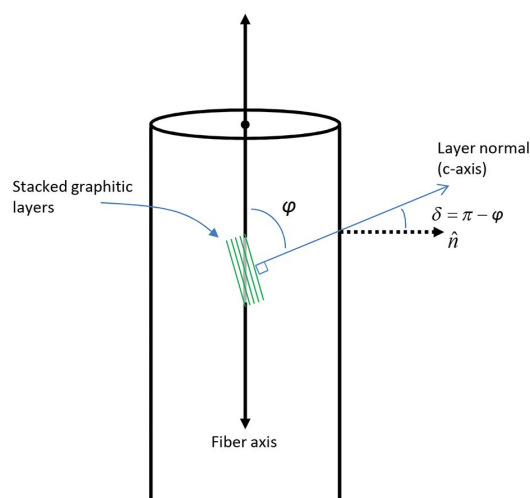
Figure 9
Schematic representation of a stacked graphitic layer domain within a carbon fibre, with orientation angles defined. Adapted from Sauder *et al.* (2004).

position in the WAXD pattern. The background position (shown in red) was chosen to correspond with the minima between peaks. As described in a previous paper (Behr *et al.*, 2016), the rigorous way of determining the background position is from the average calculated background over the predefined 2θ integration window range from an intensity slice taken along the meridional direction (along the fibre axis). However, due to the large number of WAXD patterns acquired during an *in situ* experiment, this level of analysis was impractical. Using a background that corresponds to the minima between peaks results in an overestimation of the degree of anisotropy (smaller $\langle\cos^2\varphi\rangle$) of fibres heat-treated to only moderate temperatures, thus the magnitude of changes in orientation with temperature is actually larger than the changes determined and reported herein; however, this difference is relatively minor and does not affect the conclusions drawn from *in situ* experiments.

2.7.2. Microstructural parameters d_{002}, L_c, L_a. A more complete picture of the physical changes that occur as a function of temperature can be obtained by extraction of
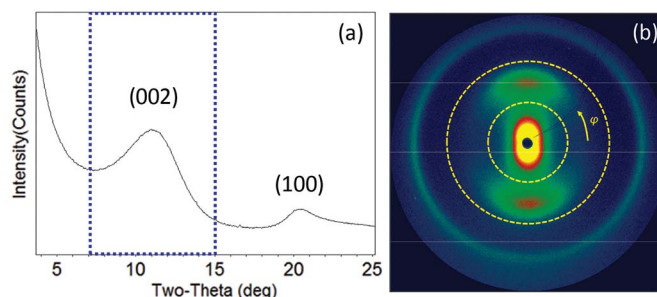
Figure 10
(*a*) Scattering intensity *versus* degrees 2θ obtained from radial integration of the WAXD pattern shown in (*b*). The blue dashed window indicates the integration width used in evaluation of the microstructure orientation. (*b*) Two-dimensional WAXD pattern from a carbon fibre with horizontal orientation. The yellow dotted circles correspond to the width of the blue box.
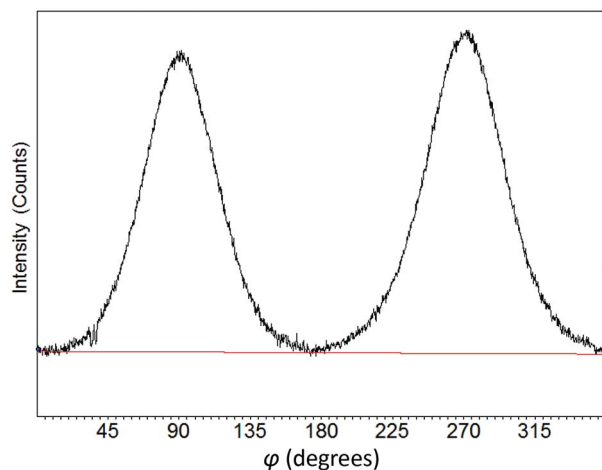
Figure 11
Azimuthal intensity variation of the (002) diffraction ring extracted from the WAXD pattern shown in Fig. 10. Azimuthal angle $\varphi = 0$ corresponds to the 3 o'clock position in the WAXD pattern. The red line is the linear background used for orientation determination.

additional microstructural characteristics of the fibre from each WAXD pattern. Specifically, three additional parameters were evaluated: the average spacing between adjacent graphitic layers, d_{002}; the average number of graphitic layers stacked together expressed as a crystal size, L_c; and the average in-plane graphitic layer size along the fibre axis, L_a. Fig. 12 shows plots of diffracted intensity *versus* degrees 2θ for slices taken along the equatorial (perpendicular to the fibre axis) and meridional (parallel to the fibre axis) directions. The intensity slice extracted along the equatorial direction exhibits three distinct peaks, which correspond to the (002), (100) and (004) graphite diffraction peaks. Along the meridional direction, the prominent peak present is (100); both the (002) and (004) peaks are largely absent due to the anisotropy of the microstructure. Microstructural parameters were extracted from each pattern after first subtracting a cubic spline background, as indicated by the red lines in Fig. 12. Pearson-VII peak shape functions with skew parameter were used to fit the observed peaks. The 2θ position and full width at half-maximum (FWHM) of the (002) peak in the equatorial slice were used to obtain d_{002} and L_c, respectively. The interlayer

spacing d_{002} was corrected for thermal expansion using the equation $d_{002} = d_{002}(T = 24°C) + 91.91 \times 10^{-6} T + 5.31 \times 10^{-9} T^2$ (Kelly, 1981). The FWHM of the (100) peak in the meridional slice was used to obtain L_a.

The crystal sizes, L_c and L_a, were extracted from the FWHM of the (002) and (100) peaks using the Scherrer formula, given by $L = (k\lambda)/(B \cos \theta_B)$, where λ is the X-ray wavelength, k is a prefactor equal to 0.9 for the (002) diffraction peak and 1.84 for the (100) diffraction peak, B is the FWHM in terms of 2θ, and θ_B is the Bragg angle in terms of θ (Jeffrey, 1971). The measured profiles of each peak were corrected for instrumental broadening by subtracting the squared resolution function width, as determined from a LaB$_6$ powder calibration standard, from the measured profile. This method has been shown to agree to within 10% of the more accurate deconvolution method, for diffraction peaks from isotactic polystyrene of similar width to the narrowest peaks observed in this work (Alexander, 1969).

2.8. Data logging and analysis

Temperature, time, input power and fibre strain are logged by two systems during an experiment: the APS Experimental Physics and Industrial Control System (EPICS), and *LabVIEW*. *LabVIEW* monitors the time, temperature, input power and fibre strain during an experiment; these data are then written to a TDM streaming (TDMS) file. The fibre strain is calculated from the change in the absolute position of the bottom clamp. The average temperature of the fibre bundle integrated over each WAXD exposure is recorded with each WAXD pattern. Rapid processing of an entire set of plot files from a single *in situ* experiment is handled *via* an Excel macro, which extracts the temperature from each plot file and outputs the data to a summary table. Since the time between consecutive WAXD patterns is known, temperature ramp rates can be easily calculated.

3. Results and discussion

Fig. 13 shows representative *in situ* data that reveal the gradual change in microstructure with increasing temperature for a
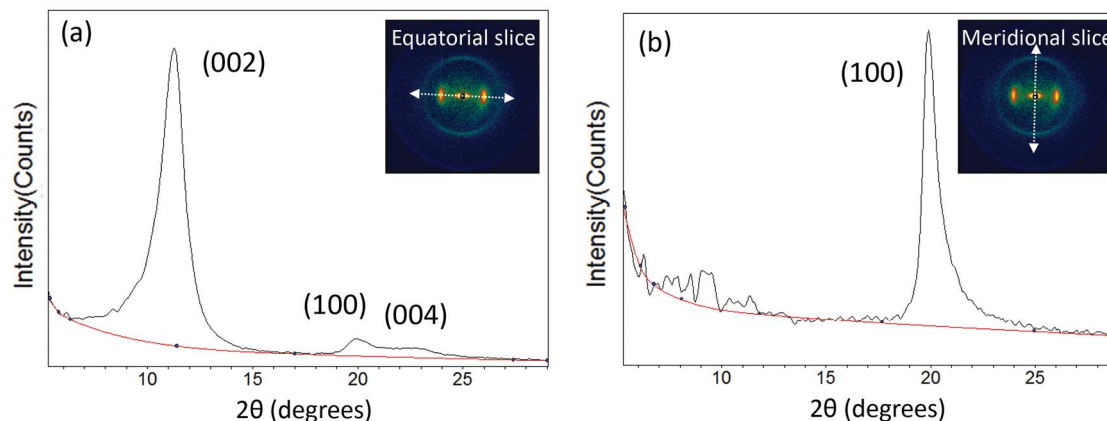
Figure 12
Intensity *versus* 2θ plots for (*a*) the equatorial slice, perpendicular to the fibre axis, and (*b*) the meridional slice, parallel to the fibre axis.

textile-grade oxidized PAN fibre. The oxidized PAN fibres were obtained from a 24k tow of textile-grade PAN precursor fibres with mean fibre diameter of 11.8 µm and standard deviation of 1.6 µm, as characterized by optical microscopy (Olympus BX51).

Specifically, the average misorientation of graphitic layers relative to the fibre axis, $\langle \cos^2 \varphi \rangle$, the average number of graphitic layers stacked together expressed as a crystal size, L_c, and the average in-plane graphitic layer size along the fibre axis, L_a, are plotted as a function of temperature. These data were obtained by heating the oxidized-PAN fibre using the surrounding tungsten coils. This material is initially characterized as possessing small crystal sizes, L_c and L_a, and a relatively well aligned microstructure.

As the temperature is increased, changes in all of the microstructural characteristics are observed as the structure transforms to the oriented graphitic microstructure of a high-modulus carbon fibre. The average misorientation of graphitic layers, described by $\langle \cos^2 \varphi \rangle$, rapidly decreases from its initial value of ~ 0.15 at 500°C to ~ 0.1 at 1100°C. Above ~ 1100°C, however, the average orientation of the layers remains largely unchanged. This plateau is consistent with the higher observed shear modulus of PAN-derived fibres, which is hypothesized to result from a higher level of covalent crosslinks connecting adjacent layers (Northolt et al., 1991). Concomitant with this decrease in misorientation is an observed sharpening of both the (100) and (200) peaks, indicating that the average in-plane graphitic layer size, L_a, and the number of stacked layers, characterized by L_c, slowly grow with temperature. L_a and L_c reach values of ~ 3 nm and ~ 2 nm, respectively, by 1750°C. It is interesting to note that this growth is delayed relative to the change in orientation, indicating that extended growth of the graphitic layers can only occur after sufficient alignment has been achieved.

In addition to temperature, the microstructure can also be affected by the magnitude of the tensile stress applied to the fibre bundle during transformation. Fig. 13 shows the impact on microstructure development in oxidized PAN fibre under high (15 MPa; solid symbols) and low (3 MPa; open symbols) stress. Although no significant effect is observed in the development of L_c and L_a, a clear decrease in the average

misorientation of graphitic layers relative to the fibre axis is observed when heating is conducted under increased tensile stress. In other words, a higher applied tensile stress reduces the temperature required to achieve a given level of microstructure orientation. Nevertheless, a plateau of orientation with increasing temperature is still reached over this temperature range for both stress levels. Determination of the stress dependence on the magnitude of this permanent microstructural change will be a focus of future study.

These results further suggest that much higher temperatures would be needed to produce the highly-aligned microstructures necessary to achieve ultra-high-modulus carbon fibres. This is consistent with the work of Isaac et al. (1994), who found that high-temperature (2700–3000°C) stretching was required to substantially increase the degree of microstructure orientation and the resulting tensile modulus of a PAN-based carbon fibre.

Indeed, investigation of microstructure evolution in PAN-derived carbon fibres at temperatures well above those achieved with coil heating, up to ~ 2300°C in this work, reveals the difficulty in overcoming this highly crosslinked structure to improve microstructure orientation. Fig. 14 shows the microstructure evolution in three commercial carbon fibres; Toray T300 (PAN-based, red triangles), Hexcel IM-7 (PAN-based, green circles) and Thornel P25 (pitch-based, black squares), over the temperature range from ~ 1250 to 2300°C. These fibres were heated in direct heating mode under 20 MPa stress to temperatures higher than those believed to be used during their manufacture. The initial microstructure of all three commercial fibres was highly oriented, a result of the combination of temperature and applied stress used during their manufacture.

Fig. 14 shows that the microstructure misorientation of all fibres decreased with increasing temperature; however, the magnitude of the observed decrease was found to depend on precursor type. The microstructure misorientation of the PAN-derived fibres, T300 and IM-7, only gradually decreases as temperature is increased from an initial $\langle \cos^2 \varphi \rangle$ value of ~ 0.093 at 1250°C to ~ 0.089 at 2250°C. In contrast, the pitch-derived P25 fibre exhibits more significant changes in microstructure orientation above a temperature of ~ 1500°C,
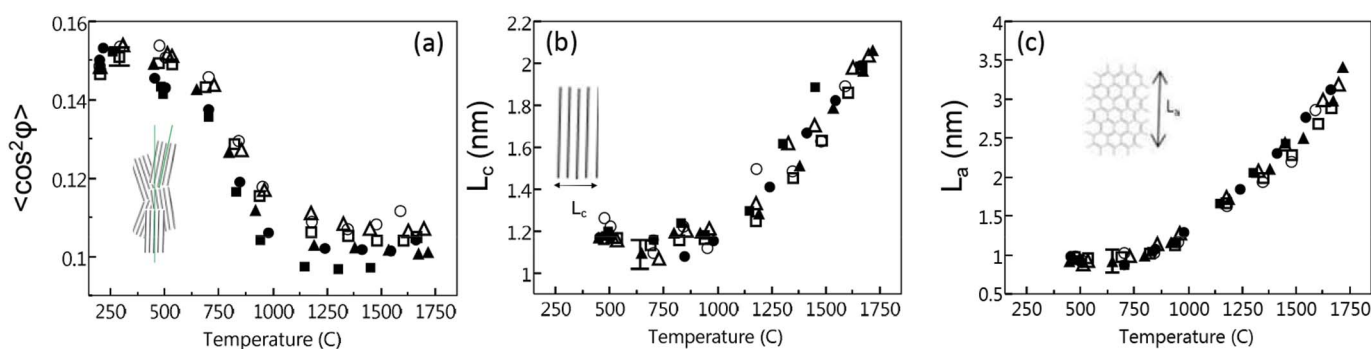
Figure 13
Microstructure orientation (a) and crystal sizes (b, c) plotted as a function of temperature from in situ tungsten coil heating experiments on oxidized PAN fibre using high (15 MPa; solid symbols) and low (3 MPa; open symbols) applied stress. Error bars were estimated from the maximum deviation between replicates.
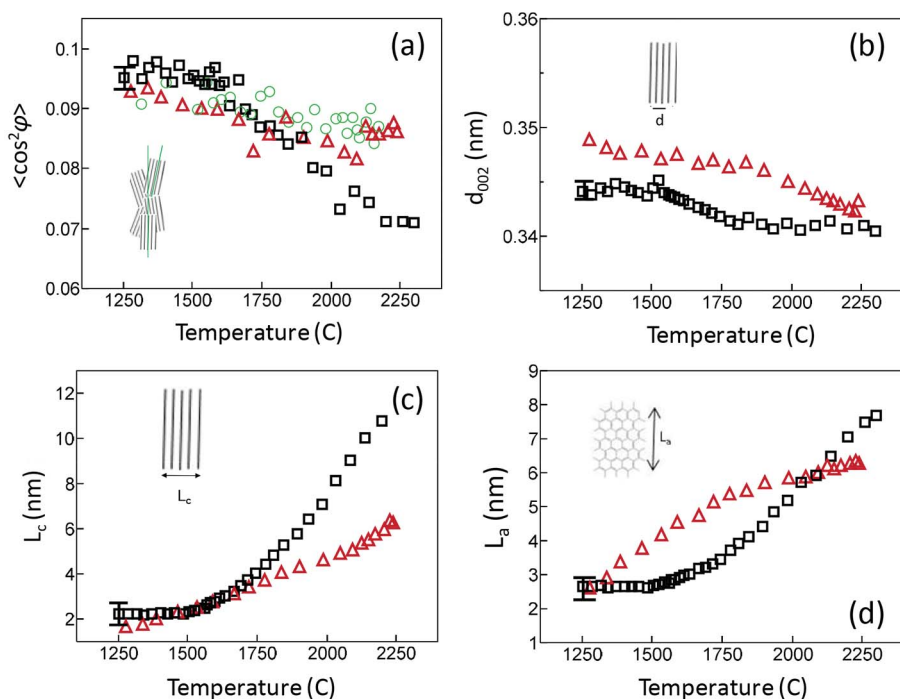
Figure 14
Microstructure orientation (*a*), *d*-spacing (*b*) and crystal sizes (*c*, *d*) plotted as a function of temperature from direct resistive heating of Toray T300 PAN (red triangles), Thornel P25 pitch (black squares) and Hexcel IM-7 PAN (green circles) carbon fibre bundles. A nominal 20 MPa stress was applied to all fibres during heating.

T300 and IM-7 fibre is not known, but is thought to also be $\sim 1500°$C.

The difference in magnitude of the observed microstructure changes with increasing temperature indicates that the graphitization behaviour for PAN- and pitch-derived carbon fibres is quite different. Indeed, this observation agrees well with previous work by Qin *et al.* (2012), who compared the properties and microstructures of PAN- and pitch-derived fibres after heat treatment with 2700°C. In general, solid C atoms are divided into two categories, *graphitizing* and *non-graphitizing* (Franklin, 1951; Jenkins & Kawamura, 1971). C atoms that form homogeneous 3D graphite structure when heated to ~ 2000–3000°C are referred to as being *graphitizable*. The relatively small change in microstructure exhibited by both PAN-derived commercial fibres is consistent with previous work by Rennhofer *et al.* (2010, 2014) and indicates that PAN is less graphitizable than pitch. Non-graphitizability of C atoms has been understood in terms of their intrinsic intertwined polymeric-like structure, high levels of covalent sp^3–sp^3 crosslinking, and the presence of curved graphitic layers (Burian *et al.*, 2002; Franklin, 1950; Harris & Tsang, 1997). These attributes are a result of the intrinsic chemical and structural properties of the precursor (Northolt *et al.*, 1991).

Previous work by our group and other researchers has shown that the modulus for shear between adjacent graphitic layers in PAN-derived carbon fibres is higher than that observed in pitch-derived fibres (Behr *et al.*, 2016; Northolt *et al.*, 1991; Sauder *et al.*, 2004). Carbon fibre derived from mesophase pitch is expected to exhibit relatively few covalent crosslinks because of the extended cyclic polyaromatic structure present in this precursor material. In contrast, PAN precursors do not contain aromatic rings. This structural difference combined with the specific oxidative stabilization processes and co-monomers used leads to high levels of crosslink formation between adjacent chains as the precursor is converted into the polyaromatic structure of carbon fibre.

changing from an initial $\langle \cos^2 \varphi \rangle$ value of ~ 0.096 at 1250°C to ~ 0.071 at 2250°C.

The average spacing between adjacent layers, d_{002}, is also observed to decrease slightly with increasing temperature. The *d*-spacing for IM-7 fibre was not evaluated. Both T300 and P25 fibres exhibit initial spacings below 0.35 nm. Upon heating, d_{002} for T300 fibre gradually decreases from its initial value of 0.349 nm at 1250°C to ~ 0.345 nm at 2250°C, whereas, for P25 fibre, d_{002} decreases from its initial value of 0.344 nm at 1250°C to ~ 0.342 nm at 2250°C.

The growth rates of in-plane layer size, L_a, and the average number of stacked layers, defined by L_c, as a function of temperature are quite different for these two fibre types. As temperature is increased, L_c for T300 is observed to increase linearly from its initial value of ~ 1.5 nm at 1250°C to ~ 6.1 nm at 2250°C, whereas L_a only initially increases linearly with temperature up to $\sim 1750°$C, and then begins to plateau, reaching a value of ~ 6.3 nm at 2250°C. In contrast, both L_c and L_a for P25 do not begin to change until the temperature reaches $\sim 1500°$C. However, above this temperature their growth rates exceed that of T300, and reach L_a and L_c values at 2250°C of 7 nm and 11 nm, respectively. Further, these values do not plateau, suggesting that this rapid growth in crystal size would continue with further increases in temperature.

The observed onset of microstructural changes for the P25 fibre at a temperature of $\sim 1500°$C suggests that this was close to the ultimate carbonization temperature used in its manufacture. The previous carbonization temperature used for

4. Conclusions

A unique high-temperature fibre tensile cell was developed to enable the investigation of carbonization and graphitization processes during conditions relevant for commercial carbon fibre production. This cell can be used to heat precursor fibre bundles to temperatures as high as $\sim 2300°$C, while applying tensile stress; the microstructure evolution as a function of temperature and time during this process is monitored by collecting real-time WAXD patterns. In this work, it was

observed that the orientation of the graphitic microstructure formed during heating in an oxidized PAN fibre could be significantly improved at temperatures up to ~1100°C while applying tensile stress; however, above this temperature the changes reached a plateau, a result of its highly crosslinked structure. Higher applied tensile stress during heating had a measureable but small effect on microstructure orientation. Commercial carbon fibres derived from PAN and pitch were further studied at higher temperatures, up to ~2300°C. Whereas the PAN-derived fibres showed little change in microstructure up to this temperature, significant changes in graphitic microstructure was observed in the pitch-derived Thornel P25 fibre. Future work will focus on the study of carbonization and graphitization behaviour of novel precursor fibre materials.

Acknowledgements

References

Alexander, L. (1969). *X-ray Diffraction Methods in Polymer Science.* New York: John Wiley and Sons, Inc.
Bacon, R. & Schalamon, W. A. (1969). *ACS Polym. Prepr.* **9**, 1338.
Behr, M. J., Landes, B. G., Barton, B. E., Bernius, M. T., Billovits, G. F., Hukkanen, E. J., Patton, J. T., Wang, W., Wood, C., Keane, D. T., Rix, J. E. & Weigand, S. J. (2016). *Carbon,* **107**, 525–535.
Burian, A. S., Koloczek, J., Dore, J. C., Honkimaki, V. & Duber, S. (2002). *Acta Phys. Pol. A,* **101**, 751–759.
Fischer, L. & Ruland, W. (1980). *Colloid Polym. Sci.* **258**, 917–922.

Franklin, R. E. (1950). *Acta Cryst.* **3**, 107–121.
Franklin, R. E. (1951). *Proc. R. Soc. A,* **209**, 196–218.
Gao, A., Su, C., Luo, S., Tong, Y. & Xu, L. (2011). *J. Phys. Chem. Solids,* **72**, 1159–1164.
Harris, P. J. F. & Tsang, S. C. (1997). *Philos. Mag. A,* **76**, 667–677.
Huang, Y. & Young, R. J. (1995). *Carbon,* **33**, 97–107.
Isaac, D. H., Ozbek, S. & Francis, J. G. (1994). *Mater. Manuf. Processes,* **9**, 179–197.
Jeffrey, J. M. (1971). *Methods in X-ray Crystallography.* New York: Academic Press.
Jenkins, G. M. & Kawamura, K. (1971). *Nature (London),* **231**, 175–176.
Johnson, D. J. (1987). *J. Phys. D,* **20**, 286–291.
Kelly, B. T. (1981). *Physics of Graphite,* pp. 196–222. London: Applied Science.
Loidl, D., Peterlik, H., Müller, M., Riekel, C. & Paris, O. (2003). *Carbon,* **41**, 563–570.
Morgan, P. (2005). *Carbon Fibres and Their Composites.* Boca Raton: Taylor & Francis.
Northolt, M. G., Veldhuizen, L. H. & Jansen, H. (1991). *Carbon,* **29**, 1267–1279.
Oberlin, A. (1984). *Carbon,* **22**, 521–541.
Ogale, A. A., Lin, C., Anderson, D. P. & Kearns, K. M. (2002). *Carbon,* **40**, 1309–1319.
Perret, R. & Ruland, W. (1970). *J. Appl. Cryst.* **3**, 525–532.
Qin, X., Lu, Y., Xiao, H., Wen, Y. & Yu, T. (2012). *Carbon,* **50**, 4459–4469.
Rennhofer, H., Loidl, D., Brandstetter, J., Kromp, K., Weiss, R. & Peterlik, H. (2006). *Fatigue Fracture Eng. Mater. Struct.* **29**, 167–172.
Rennhofer, H., Loidl, D., Puchegger, S. & Peterlik, H. (2010). *Carbon,* **48**, 964–971.
Rennhofer, H., Puchegger, S., Pabisch, S., Rentenberger, C., Li, C., Siegel, S., Steiger-Thirsfeld, A., Paris, O. & Peterlik, H. (2014). *Carbon,* **80**, 373–381.
Rudolf, P. R. & Landes, B. G. (1994). *Spectroscopy,* **9**, 22–33.
Ruland, W. (1968). *ACS Polym. Prepr.* **9**, 1368–1375.
Sauder, C., Lamon, J. & Pailler, R. (2002). *Compos. Sci. Technol.* **62**, 499–504.
Sauder, C., Lamon, J. & Pailler, R. (2004). *Carbon,* **42**, 715–725.
Wu, G. P., Li, D. H., Yang, Y., Lu, C., Zhang, S. C., Li, X. T., Feng, Z. H. & Li, Z. H. (2011). *J. Mater. Sci.* **47**, 2882–2890.
Zhao, H., Min, K. & Aluru, N. R. (2009). *Nano Lett.* **9**, 3012–3015.
Zhou, G., Liu, Y., He, L., Guo, Q. & Ye, H. (2011). *Carbon,* **49**, 2883–2892.